ACS APPLIED MATERIALS & INTERFACES

Research Article

www.acsami.org

Harnessing Denatured Protein for Controllable Bipolar Doping of a Monolayer Graphene

Sung Kyu Jang,[†,‡] Ji-ryang Jang,[†,‡] Woo-Seok Choe,*[,†,§] and Sungjoo Lee*[,†,⊥,∥]

[†]SKKU Advanced Institute of Nanotechnology (SAINT), [§]School of Chemical Engineering, and [∥]College of Information and Communication Engineering, Sungkyunkwan University (SKKU), Suwon 440-746, Korea

[⊥]Center for Human Interface Nanotechnology (HINT), Suwon 440-746, Korea

ABSTRACT: In this work, we demonstrated tunable p- and/or n-type doping of chemical vapor deposition-grown graphene with the use of protein bovine serum albumin (BSA) as a dopant. BSA undergoes protonation or deprotonation reaction subject to solution pH, thereby acting as either an electron donor or an electron acceptor on the graphene surface layered with denatured BSA through π-stacking interaction. This direct annealing of graphene with denatured BSA of amphoteric nature rendered facilitated fabrication of a p- and/or n-type graphene transistor by modulating pH-dependent net charges of the single dopant. Following AFM confirmation of the BSA/graphene interface assembly, the carrier transport properties of BSA-doped graphene transistors were assessed by $I-V$ measurement and Raman spectra to show effective charge modulation of the graphene enabled by BSA doping at various pH conditions. The protein-mediated bipolar doping of graphene demonstrated in our work is simple, scalable, and straightforward; the proposed scheme is therefore expected to provide a useful alternative for fabricating graphene transistors of novel properties and promote their implementation in practice.

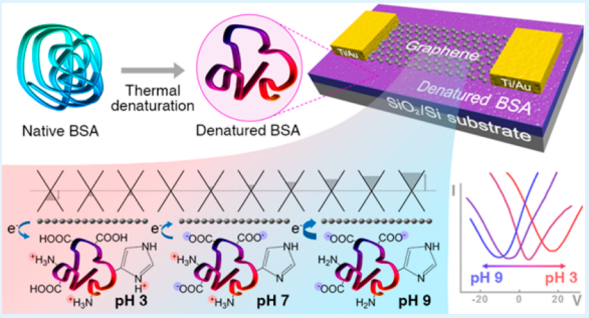

KEYWORDS: *graphene, bipolar doping, protein, heat-denaturation*

INTRODUCTION

Graphene, a two-dimensional allotrope of carbon, has demonstrated great promise for electronic technology and fundamental physics applications because of its superior properties.[1−3] To fully realize its potential for electronic device applications, graphene should display both p- and n-type conductance; it should also have the ability to control the carrier density in order to provide active functionalities in the devices. Surface adsorption and edge decoration have been used to provide p- and n-type doping. Unfortunately, the molecules used in these processes, such as NH_3, alkali atoms, and NO_2, can introduce dimer bonds, which may exert adverse effects on electronic device operation.[4−6] Alternatively, charge-transfer doping can modulate the carrier density with minimal defects and impairment of graphene structure. The adsorption of various organic molecules has been used to dope graphene films,[7−9] but it remains challenging to accurately control the adsorption coverage and the carrier concentration. Moreover, many of the existing methods present complications and/or side effects that limit their applications. For example, different molecules are required to control the type (hole vs electron) and concentration of the charge carrier, and the chemical dopants are toxic and hence not suitable for biological applications. To address these issues, the use of proteins as a dopant has been explored by virtue of their pH-dependent ionization and electrochemical properties. Protein molecules exhibit either positive or negative net charges following their ionization at a given pH departing from their isoelectric points.[10] It was shown that protein molecules could interact electrostatically, when pH and electrochemical potential were controlled, with various metal- and carbon-based electrodes including graphene, and the protein molecules subsequently undergo rearrangement on the electrode surface to form stable protein−electrode complexes.[11−13] Furthermore, protein molecules atop the electrodes were found to produce voltammetric peaks attributed primarily to the presence of electroactive amino acid residues (e.g., Tyr, Trp, and Cys) capable of providing a charge-transfer channel through their electrochemical oxidation.[12−16] It is also interesting to note that denatured proteins largely accounted for higher current values than the corresponding proteins in native forms when subjected to electrochemical oxidation on the mercury and/or carbon electrode,[13,17] presumably due to the increased availability of electroactive hydrophobic amino acid residues at the protein−electrode interface. Besides, it was shown that a denatured state of the protein molecule was conducive, via enhanced π-stacking interaction, to protein layer formation on hydrophobic surfaces such as mercury, carbon, and graphene.[13,17,18] In order to further explore the potential of exploiting protein as a charge-transfer modulator in fabrication of protein-doped graphene

Received: October 22, 2014
Accepted: December 29, 2014
Published: December 29, 2014

DOI: 10.1021/am507246v
ACS Appl. Mater. Interfaces 2015, 7, 1250−1256

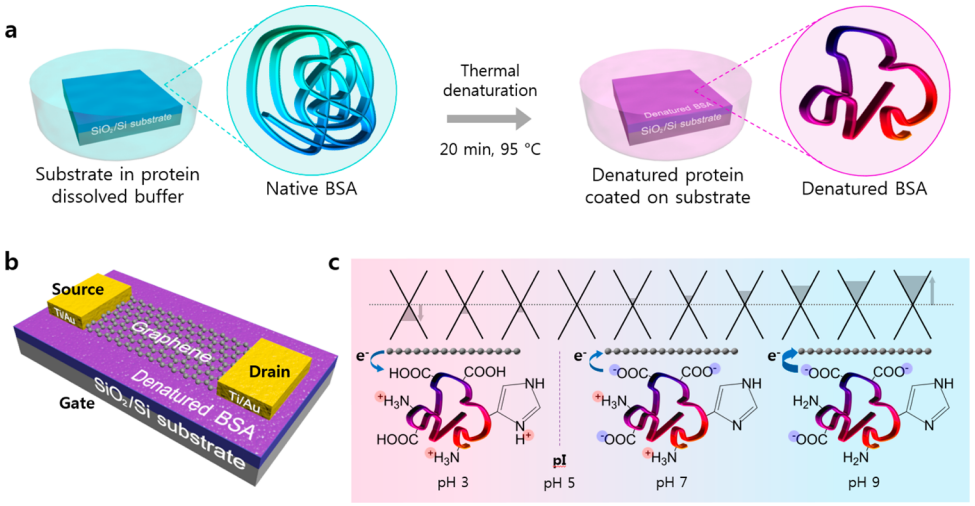

Figure 1. Schematics of the protein coating process mediated by π-stacking interaction between thermally denatured BSA and the substrate (a), field-effect transistors (FETs) using BSA-doped graphene (b), and putative alteration of graphene band structure effected by charge transfer from BSA layers at different pH (c).

transistor, herein, we report an alternative graphene doping method where charge is transferred from denatured bovine serum albumin (BSA) layers to the graphene surface in a pH-controlled manner. This method has the advantage of continuous modulation of carrier densities without degradation of the graphene film. The graphene films used in this work were prepared by chemical vapor deposition (CVD) and directly annealed with the SiO_2 substrate layered with heat-denatured BSA to give rise to a novel graphene transistor in graphene/protein/SiO_2 sandwich structure. The effects of charge-transfer doping afforded by pH-controlled denatured BSA layers on the performance of BSA-doped graphene transistor were investigated using Raman spectroscopy and electrical measurement.

EXPERIMENTAL SECTION

Heavily p-doped silicon substrates (0.05 ohm cm) with 300 nm SiO_2 were cleaned consecutively with acetone, isopropyl alcohol, and deionized water by ultrasonication for 10 min each at room temperature. The substrates were then treated with piranha solution (98% H_2SO_4:30% H_2O_2 = 3:1 in volume) for 15 min, followed by rinsing with deionized water. Each cleansed substrate was placed in 10 mL of various concentrations of BSA (Sigma-Aldrich, USA) dissolved in 20 mM acetate (pH 3), 20 mM Tris (pH 7), and 20 mM Tris (pH 9) buffers. The solution containing SiO_2 substrate was incubated for 6 h at 25 °C for adsorption of native BSA on SiO_2 surface or incubated for 20 min at 95 °C for adsorption of denatured BSA on SiO_2 surface (Figure 1a). For measurement of the thickness of the protein layer, SiO_2 substrate partially coated with photoresistor was incubated with 10 mL of 1×10^{-4} M BSA dissolved in 20 mM acetate (pH 3), 20 mM Tris (pH 7), or 20 mM Tris (pH 9) for 20 min at 95 °C. Following BSA deposition, the thickness profile was obtained using an atomic force microscope (AFM) (INNOVA, Veeco Inc.).

Graphene films were synthesized using the CVD method. A copper foil was placed in the center of the tube and then heated to 1000 °C in 80 mTorr of H_2 flowing at 10 sccm. After reaching 1000 °C, the sample was annealed for 30 min at the same H_2 flow rate and pressure in order to polish the copper substrate, increase the grain size, and yield high-quality graphene films.[19] CH_4 and H_2 gases were then introduced at rates of 20 and 10 sccm, respectively, for 30 min to grow continuous graphene in a CH_4/H_2 mixture at a total pressure of 300 mTorr. Finally, the sample was cooled to room temperature in H_2 flowing at 10 sccm and 80 mTorr. The monolayer nature of the grown graphene film was confirmed by AFM and Raman spectra analysis. The graphene-coated Cu foil was spin coated with a poly(methyl methacrylate) (PMMA) film and etched by an ammonium persulfate aqueous solution (40 g/L) overnight. Etching was followed by a 10 min rinse in ultrapure water for cleaning. The PMMA/graphene film was then placed onto the target substrate and dried in air for 1 h. The sample was then immersed in cold acetone for 10 min to dissolve the PMMA. The graphene films were transferred onto denatured BSA-deposited substrates for further evaluation and subsequent transistor fabrication. The field-effect transistors (FET) were fabricated by using photolithography, electron-beam evaporation, and a metal lift-off process. Ti/Au (5/60 nm thick) source and drain electrodes were patterned on graphene films. The channel was defined by photolithography, and the surrounding graphene was etched by O_2 RIE plasma at 470 mTorr and 20 W. The channel dimensions of these transistors are 5 μm in width and 10 μm in length. The fabricated device structure is shown in Figure 1b. After the fabrication, we determined their electrical characteristics using a semiconductor parametric analyzer (Keithley 4200, Keithley Instruments Inc.).

RESULTS AND DISCUSSION

The rationale behind the use of bovine serum albumin (BSA) in the present study for fabrication of graphene transistor is two-fold: one as a charge modulating dopant in a pH-dependent manner and the other as an effective interfacial adhesive capable of annealing heterogeneous surfaces lacking direct compatibility (e.g., graphene and SiO_2) in a structure-dependent manner (more details will be provided later).[18]

Proteins consist of long chains of amino acids, but the amino acid compositions and sequences of individual proteins differ from one another. Since some of the amino acid residues such as Arg, His, Lys, Asp, and Glu are differentially protonated or deprotonated at a given pH when existing in a protein chain, all proteins including BSA exhibit either positive or negative net charges at pH values departing from their isoelectric points (pI). Therefore, a protein molecule can serve as either an electron donor or an electron acceptor by leveraging the pH at the time of graphene doping. BSA has a pI between pH 4.7 and 5.2,[10] indicating that it is almost neutrally charged at pH 5. Lowering the pH from 5 to 3 results in BSA becoming positively charged via protonation of the carboxyl groups (i.e., the conversion of $-COO^-$ into $-COOH$) of aspartic and glutamic acids. Increasing the pH from 5 to 7, on the other hand, results in BSA becoming net negatively charged due to the loss of protons from the imidazole groups of histidines.

DOI: 10.1021/am507246v
ACS Appl. Mater. Interfaces 2015, 7, 1250−1256

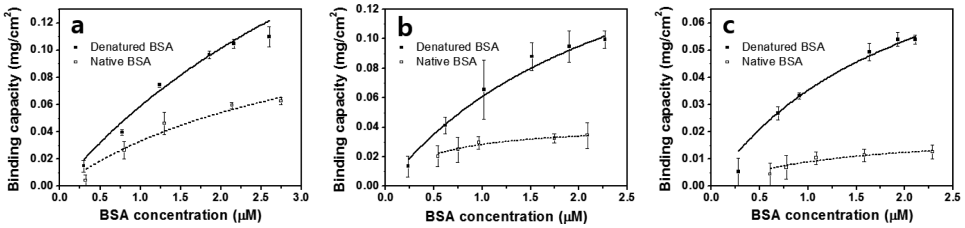

Figure 2. Batch adsorption isotherms for native and denatured BSA binding to SiO_2 surface at pH 3 (a), 7 (b), and 9 (c). Solid and dashed lines were fitted using the Langmuir adsorption model. Data are presented as mean ± standard deviation (n = 3).

When the pH is raised from 7 to 9, BSA becomes even more negatively charged because of further loss of protons from the ammonium groups of lysines (i.e., the conversion of $-NH_3^+$ into $-NH_2$) and from the guanidinium groups of arginines.[10,20] This process is summarized in Figure 1c. As a result, the charge of a BSA layer could be controlled by changing the solution pH.

On SiO_2 surface, hydrophobic (siloxane, Si−O−Si) and hydrophilic (silanol, Si−OH) groups coexist.[21] Therefore, BSA adsorption to SiO_2 is likely to be mediated by both hydrophobic and hydrophilic interactions. On the other hand, since graphene surface comprising only carbon atoms is extremely hydrophobic, the abundant presence of hydrophobic amino acid residues on the exterior of BSA (often triggered by protein denaturation) allowing for π-stacking interaction between graphene and protein layers[18] is critical for the adhesive anchoring of protein-coated SiO_2 to graphene surface. This led us to consider first what protein structure (i.e., native vs denatured) would be more conducive to fabricating the graphene transistor depicted in Figure 1b. The adsorption of native and denatured BSA to SiO_2 was therefore tested at various pH conditions to assess structure-dependent binding behavior of BSA to SiO_2. Out of the two most widely employed protein denaturation methods (i.e., chemical and heat treatment), the heat-denaturation method was used in this study for BSA denaturation in order to avoid any potential intervening effect arising from the presence of chaotropic denaturants and reducing agents often required for chemical denaturation on hydrophobic interaction between the denatured BSA and the substrate. Furthermore, in comparison with the chemically denatured BSA, heat-denatured BSA was found to be superior for passivating the hydrophobic surface with an almost complete coverage to give uniform and smooth protein layers.[18] Also, the presence of hydrophobic substrate (i.e., SiO_2), at the time of thermal denaturation of BSA, allowed more denatured BSA molecules to preferentially interact via phi-stacking with the SiO_2 surface during a short incubation period of 20 min while suppressing the self-aggregation between the denatured BSA molecules. However, when the incubation time was prolonged for more than 30 min, the unbound denatured BSA molecules were found to form insoluble coagulates in solution. Hence, the substrate passivation with heat-denatured BSA was terminated after 20 min prior to encountering protein aggregates and/or coagulates. As shown in Figure 2, when native BSA was bound to SiO_2 surface in the acidic pH region (i.e., pH 3), electrostatic attraction mainly occurred between positively charged BSA and negatively charged SiO_2 surface with the pIs of BSA and SiO_2 being 5 and 1, respectively.[22] On the other hand, native BSA adsorption to SiO_2 decreased in the alkaline pH region (i.e., pH 7 and 9) because of electrostatic repulsion between negatively charged BSA and SiO_2 surface in addition to the decrease in hydrophobic interaction as a result of increased hydrophilicity of the protein due to titration of acidic groups.[23] Using the Langmuir model based nonlinear regression analysis of the adsorption data shown in Figure 2, maximum binding capacities (Q_{max}) for the native BSA binding to SiO_2 at pH 3, 7, and 9 were determined to be 0.15, 0.04, and 0.02 mg/cm^2, respectively. For the heat-denatured BSA adsorption, the adsorption isotherms showed a similar trend as for the native BSA. However, the amount of denatured BSA adsorbed to SiO_2 surface at each pH condition (Q_{max} at pH 3, 7, and 9 is 0.36, 0.22, and 0.11 mg/cm^2, respectively) was significantly larger than that for native BSA. This is probably due to the increased hydrophobic and/or London−van der Waals interactions between siloxane groups on SiO_2 surface and outwardly relocated bulky hydrophobic amino acid residue patches populated in denatured BSA following heat treatment.[24]

As deduced from the binding behavior of native and denatured BSA on SiO_2 surface at varying pH conditions, the use of denatured BSA would be superior to native BSA in view of providing a larger pool of protein molecules capable of acting as electron donors/acceptors on the substrate surface in a pH-dependent manner. Furthermore, denatured BSA proved to be more conducive than native BSA to seamless interfacing of graphene with protein layers on SiO_2 with enhanced passivation efficiency,[18] which is critical to avoid severe charge fluctuations often resulting from unintended localized doping of graphene surface. On the basis of these 2-fold merits afforded by denatured BSA as above, it was therefore decided to use the denatured form of BSA as a charge-modulating dopant and also as an anchoring agent for assembly of protein-intervened graphene/SiO_2 sandwich structure required for construction of graphene transistor shown in Figure 1b.

In order to ensure a uniform and complete surface coverage of both SiO_2 and graphene surfaces with protein layers, all subsequent experiments for preparation of BSA-coated SiO_2 were conducted using 10^{-4} M denatured BSA, which is at least 20 times higher than the dissociation constants (K_d of 5.1, 2.6, and 2.1 μM) estimated for denatured BSA binding to SiO_2 at pH 3, 7, and 9, respectively (Figure 2). At this elevated concentration, the amount of denatured BSA adsorbed to SiO_2 was significantly higher (0.91 ± 0.04, 0.88 ± 0.02, and 0.75 ± 0.04 mg/cm^2 at pH 3, 7, and 9, respectively) than its Q_{max} determined previously at each pH condition, indicative of the formation of multilayered protein matrices. It is reckoned that the surface density of denatured BSA to form a single layer of protein molecules with almost complete passivation of the substrate surface could be approximated to 0.3 mg/cm^2 based on the Q_{max} determined for denatured BSA binding to SiO_2 at pH 3 (i.e., the most favorable pH condition tested to maximize protein binding). This implies that denatured BSA molecules at an initial concentration of 10^{-4} M stack on one another on SiO_2 surface and undergo layer-by-layer assembly to apparently

DOI: 10.1021/am507246v
ACS Appl. Mater. Interfaces 2015, 7, 1250−1256

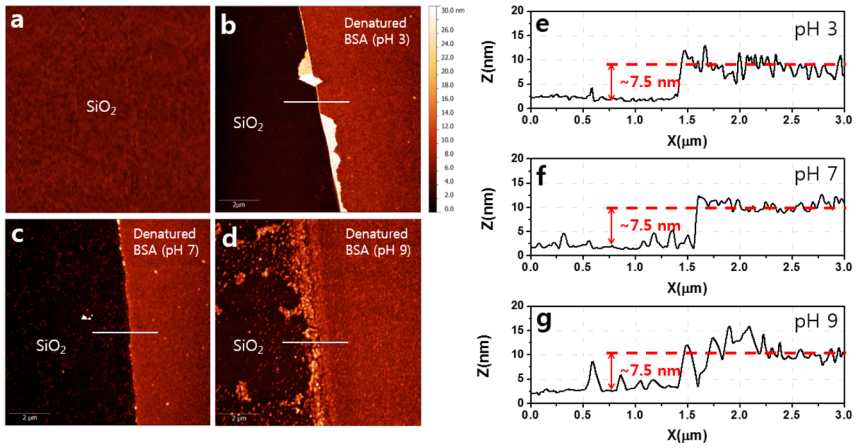

Figure 3. AFM images of bare SiO_2 (a) and SiO_2 layered with denatured BSA at pH 3 (b), 7 (c), and 9 (d). To assess the thickness of protein layers on SiO_2 with reference to bare SiO_2 surface at each pH condition, patterned substrate surfaces comprising bare SiO_2 next to protein-coated SiO_2 region were prepared by photolithography at each pH. The thickness of BSA layer is around 7.5 nm regardless of pH (e–g) when measured along the horizontal white lines indicated in the AFM images (b–d).

give rise to a protein matrix in three-layer configuration at pH 3. It is also interesting to note that the number of protein layers in the protein matrix formed at pH 7 or 9 is close to three despite the small Q_{max} to account for the less efficient formation of a BSA monolayer of low density at high pH. This is because stacking of adjacent layers atop the already-formed first layer is likely to experience less electrostatic repulsion directly exerted by highly negatively charged SiO_2 surface at high pH.

The surface topography of the protein-coated substrate and the thickness of protein layer were also characterized by AFM measurement. AFM images of protein-free and BSA-coated substrates are shown in Figure 3a–d. The values measured for the RMS surface roughness of bare and BSA-coated SiO_2 at pH 3, 7, and 9 were 0.20, 0.51, 0.61, and 0.33 nm, respectively. These results show that denatured BSA molecules were evenly layered on the SiO_2 substrate. Besides, thicknesses of the BSA matrices prepared at different pH were very similar to one another as shown in Figure 3e–g. The estimated three-layer configuration of the denatured BSA matrix on SiO_2 was confirmed by comparison with the thickness of a protein monolayer determined by AFM analysis which was found to be 2.39 ± 0.34 nm (data not shown). It is reckoned that hydrophobic interaction and electrostatic repulsion are dominant among the denatured protein molecules at a given pH. Even though the extent of electrostatic repulsion will vary in a pH-dependent manner, the major interaction experienced by the denatured protein molecules is of hydrophobic nature due to the abundance of hydrophobic patches outwardly exposed on the protein surface upon denaturation. This often renders the denatured protein molecules prone to aggregation despite the presence of electrostatic repulsion regardless of pH and accounts for the similar height of protein matrices on SiO_2 despite the pH difference as shown in Figure 3e–g.

In summary, it was confirmed that multilayer denatured protein matrix could be formed on SiO_2 surface using denatured BSA with more or less the same efficiency in a broad pH range. Importantly, denatured BSA matrices assembled on SiO_2 at different pH showed no remarkable differences in view of layer roughness, thickness, and structure, despite the clearly distinctive binding behavior of denatured BSA against SiO_2 as evidenced by pH-dependent large variations in Q_{max} and K_d, when the protein concentration used for layer formation was dozens-fold higher than K_d values. This would negate the possibility that topological change in the protein matrices prepared at different pH per se may directly affect electrical performance of SiO_2-supported graphene transistor. Furthermore, the use of BSA in denatured form is critical for efficient adhesion of CVD-grown graphene with protein-layered SiO_2 to fabricate a transistor device.[18,25] This is because hydrophobic amino acid residues actively participating in π-stacking interactions with graphene surface are readily available at the exterior of protein upon its denaturation which would otherwise be mostly buried inside protein globule. The assembly of uniform multilayered protein matrix on SiO_2 in a pH-independent manner is thus expected to provide a useful scaffold for stable interfacing of protein-coated SiO_2 with monolayer graphene film and subsequent bipolar doping with the use of a large amount of matrix-embedded protein molecules as an adhesive agent as well as electron/hole generator.

Following fabrication of the graphene transistor device as shown in Figure 1b according to the procedure detailed in the Experimental Section, Raman spectroscopy and electrical measurement were conducted to investigate the effects of protein-mediated charge-transfer doping on the graphene.

Raman spectroscopy has been shown to be a powerful technique for monitoring the number of layers, disorder, and doping of graphene.[26,27] The Raman G band is especially sensitive to doping and provides useful information to determine whether n- or p-type doping of graphene takes place. Figure 4a shows the Raman G band profiles of graphene interfaced with BSA-coated and BSA-free SiO_2. For simplicity, graphene interfaced with BSA-layered SiO_2 prepared at pH 3, 7, and 9 is designated hereafter as BSA-pH3, BSA-pH7, and BSA-pH9 graphene, respectively; graphene interfaced with bare SiO_2 is designated as BSA-free graphene. The frequency of the G band for graphene is affected by the extent of its interaction with electron donors or acceptors. While the G band downshifts for n-doped graphene, it upshifts for p-doped graphene.[8,9] Since denatured BSA molecules are negatively charged at pH 7 and 9, they work as electron donors. The Raman G band peak frequencies of BSA-pH7 and BSA-pH9 graphene were measured to be 1580 and 1576 cm^{-1}, downshifted by 4 and 8 cm^{-1} from that of BSA-free graphene

DOI: 10.1021/am507246v
ACS Appl. Mater. Interfaces 2015, 7, 1250–1256

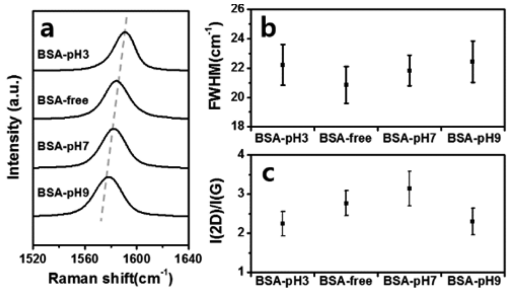

Figure 4. Raman spectra of BSA-free graphene and graphene layers doped with denatured BSA at different pH. Individual Raman spectra of the G band of the graphene layers following their interfacing with BSA-free and BSA-coated SiO_2 are shown with a dotted line to show pH-dependent Raman shift (a). The fwhm of the G band (b) and the intensity ratio of the 2D/G band (c) of graphene layers following their interfacing with BSA-free and BSA-coated SiO_2 are shown with error bars representing the standard deviations for independent measurements repeated three times. Note that the graphene on BSA-free SiO_2 was slightly p-doped by ambient adsorbates. The fwhm of the G band increased and the intensity of the 2D/G band decreased with doping of graphene.

(1584 cm^{-1}). In contrast, BSA works as an electron acceptor at pH 3, and the G band frequency of BSA-pH3 graphene was found to be 1592 cm^{-1}, upshifted by 8 cm^{-1} from that of BSA-free graphene. The ratio of the intensities of the Raman 2D and G bands, $I(2D)/I(G)$, and full width at half-maximum (fwhm) of the G band also provide useful criteria to determine the amount of doping. As shown in Figure 4b, the fwhm of G band values measured for BSA-pH3, BSA-pH7, and BSA-pH9 graphene are 22.22 ± 1.39, 21.84 ± 1.04, and 22.44 ± 1.43 cm^{-1}, respectively, as compared to 20.84 ± 1.26 cm^{-1} for BSA-free graphene. The fwhm of the G band was found to increase for both types of doping, consistent with the trend reported elsewhere.[8] As shown in Figure 4c, the $I(2D)/I(G)$ ratio obtained from BSA-pH7 graphene exhibited a maximum value of 3.14 ± 0.44, whereas the ratios for BSA-pH3, BSA-pH9, and BSA-free graphene were 2.24 ± 0.31, 2.31 ± 0.34, and 2.77 ± 0.32, respectively. The decrease in the $I(2D)/I(G)$ ratio for both hole and electron doping is consistent with previous studies[8,28] considering that the graphene on SiO_2 is slightly p-doped by ambient adsorbates.[29]

Figure 5a shows the charge-transfer characteristics (drain current I_d vs gate voltage V_g) of field-effect transistors fabricated

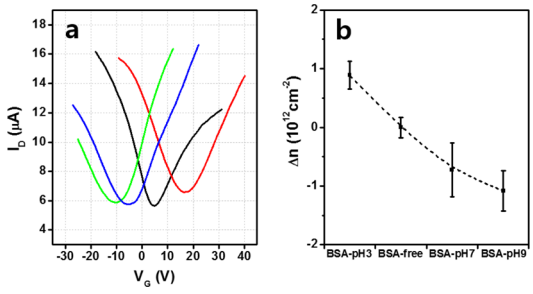

Figure 5. $I-V$ curves to show electrical performance of the BSA-pH3 (red), BSA-pH7 (blue), and BSA-pH9 (green) graphene FETs with reference to the BSA-free graphene FET (black) (a). Profile to show the change in the induced carrier concentrations (Δn) for the graphene FETs (b). These clearly showed that charge-transfer doping of graphene with denatured BSA was significantly affected by the pH at the time of denatured BSA layer assembly.

with graphenes with or without BSA. The measurement was conducted in a vacuum (5×10^{-6} Torr) at room temperature. We compared the Dirac points (V_{Dirac}, the gate voltage corresponding to the minimum conductivity) of various graphene transistors to investigate the doping effects by BSA at different pH. The BSA-free graphene transistors exhibited almost symmetric $I-V$ curves, with a Dirac point of 4.94 ± 1.21 V. In the presence of BSA layers intervening between graphene and the SiO_2, the Dirac points of the BSA-doped graphene transistors shifted toward negative or positive voltages depending on the pH at the time of BSA deposition. BSA-pH3 graphene transistor exhibited p-doped transport behavior with the Dirac point of 17.4 ± 1.65 V. On the other hand, BSA-pH7 and BSA-pH9 graphene transistors exhibited n-doped transport behaviors with Dirac points of −5.31 ± 2.83 and −10.27 ± 2.41 V, respectively. In order to calculate the carrier concentration induced by protein-mediated charge-transfer doping, the following relationship between the Dirac point (V_{Dirac}) and carrier concentration (n) was used

$$V_{Dirac} = \frac{\hbar|v_F|\sqrt{\pi n}}{e} + \frac{ne}{C_{ox}}$$

Using the values of the reduced Planck constant ($\hbar = 6.58 \times 10^{-16}$ eV·s), Fermi velocity ($v_F = 1 \times 10^6$ m·s^{-1}),[2,3] gate capacitance ($C_{ox} = 1.15 \times 10^{-4}$ F·m^{-2}), and electron charge ($e = 1.6 \times 10^{-19}$ F·V), the relationship was simplified to

$$V_{Dirac} = 1.17 \times 10^{-7}\sqrt{n} + 1.391 \times 10^{-11} n$$

From this equation, the carrier concentration for BSA-free graphene FET was calculated to be 3.50×10^{11} cm^{-2} (n_0), presumably via interaction with ambient adsorbates.[29] As shown in Figure 5b, the carrier concentrations induced for protein-doped graphene FETs with reference to the BSA-free case ($\Delta n = n - n_0$) were found to range from -1.1×10^{12} to 0.9×10^{12} cm^{-2} depending on the pH used for denatured BSA deposition. This implies that the carrier concentration of graphene can be controlled by concentration- and pH-dependent net charge of protein molecules. Carrier concentration should be related to the amount of dopant (i.e., denatured BSA molecules intervening between graphene and SiO_2 surfaces) and the amount of charges of varying polarity available at a given pH. When the protein adsorption onto the substrate occurs at low concentrations unable to achieve Q_{max}, the doping effect should consider the amount of the proteins adsorbed and available charges at a given pH on the substrate surface. This is especially important if the protein layer formed on the substrate exists in a monolayer where Q_{max} in Langmuir isotherm specifies the maximum availability of protein to work as a dopant and thereby to affect carrier concentration. However, in this study, the amounts of adsorbed proteins on the SiO_2 surface were significantly higher than the estimated Q_{max} since protein adsorption was conducted at 10^{-4} M (i.e., at least 20 times higher than K_d) as described earlier. In addition, thicknesses of the denatured BSA matrices formed at different pH were very similar to one another, indicative of the availability of similar amounts of denatured BSA regardless of pH at the interface between graphene and SiO_2. This suggests that Q_{max} determined for denatured BSA adsorption at different pH conditions does not specify the maximum carrier doping concentration. Rather, pH-modulated charge polarity and their amount are the key players in determining carrier doping effects. After confirming that BSA-mediated charge-transfer

DOI: 10.1021/am507246v
ACS Appl. Mater. Interfaces 2015, 7, 1250−1256

doping could effectively modulate the graphene property in view of doping type and carrier concentration as discussed above, it is tempting to understand how this protein-mediated doping may perturb the charge carrier flow. The field effect mobility was thus estimated using the following equation

$$\mu = \frac{L}{W}\frac{1}{C_{OX}V_{ds}}\Delta g_m$$

where L is the channel length (μm), W the channel width (μm), C_{ox} the gate capacitance ($F \cdot m^{-2}$), V_{ds} the source-drain voltage (V), and Δg_m the differential transconductance ($I \cdot V^{-1}$). The field effect mobility for each graphene transistor was found to exist between 950 and 1400 $cm^2\ V^{-1} \cdot s^{-1}$, indicative of no apparent significant mobility degradation implicated with protein-mediated doping. Taken together, these results show that the use of denatured BSA for graphene doping provides an effective yet simple strategy to modulate the electrical properties of graphene without compromising the device performance.

CONCLUSIONS

We demonstrated a novel method to dope graphene using denatured BSA layered on SiO_2 prior to its interfacing with graphene in order to fabricate an FET in SiO_2/BSA/graphene sandwich structure. Heat-treated BSA was shown to assemble on SiO_2 to give a smooth and thick multilayer protein matrix of differential charge polarity at varying pH. BSA in denatured form whose exterior is enriched with hydrophobic amino acid residues enabled efficient pH-modulated bipolar doping of CVD-grown monolayer and stable adhesion of the graphene film to the transistor device by providing a large pool of protein molecules intervening SiO_2 and graphene surfaces. Raman spectroscopy and electrical analysis confirmed that the fabricated SiO_2/BSA/graphene FET showed the signature behavior of p- and/or n-doped graphene with varying amounts of induced carriers subject to pH without compromising electrical performance often accompanied by postdoping degradation of field effect mobility. Overall, the use of denatured protein with simple pH adjustment proved to be a useful platform technology for bipolar doping of graphene for modulating electrical properties of graphene. Harnessing other proteins of diversified properties in place of BSA would also be promising in view of producing high-quality graphenes of more diversified properties.

AUTHOR INFORMATION

Corresponding Authors

*E-mail: checws@skku.edu.
*E-mail: leesj@skku.edu.

Author Contributions

‡These authors contributed equally to this work.

Notes

The authors declare no competing financial interest.

ACKNOWLEDGMENTS

This research was supported by the Pioneer Research Center Program through the National Research Foundation of Korea funded by the Ministry of Science, ICT & Future Planning (2014M3C1A3053024), and Basic Science Research Program through the National Research Foundation of Korea funded by the Korean government (MSIP) (grant nos. 2009-0083540, 2012R1A1A2020089, and 2012M1A2A2671795), and Global Frontier Program through the Global Frontier Hybrid Interface Materials (GFHIM) (2013M3A6B1078873) of the National Research Foundation of Korea (NRF) funded by the MOSIP, Korea.

REFERENCES

(1) Geim, A.; Novoselov, K. The Rise of Graphene. *Nat. Mater.* **2007**, 183−191.
(2) Novoselov, K. S.; Geim, A. K.; Morozov, S. V.; Jiang, D.; Katsnelson, M. I.; Grigorieva, I. V.; Dubonos, S. V.; Firsov, A. A. Two-dimensional Gas of Massless Dirac Fermions in Graphene. *Nature* **2005**, *438*, 197−200.
(3) Zhang, Y.; Tan, Y.-W.; Stormer, H. L.; Kim, P. Experimental Observation of the Quantum Hall Effect and Berry's Phase in Graphene. *Nature* **2005**, *438*, 201−204.
(4) Zhou, S. Y.; Siegel, D. A.; Fedorov, A. V.; Lanzara, A. Metal to Insulator Transition in Epitaxial Graphene Induced by Molecular Doping. *Phys. Rev. Lett.* **2008**, *101*, 86402.
(5) Wang, X.; Li, X.; Zhang, L.; Yoon, Y.; Weber, P. K.; Wang, H.; Guo, J.; Dai, H. N-Doping of Graphene Through Electrothermal Reactions with Ammonia. *Science* **2009**, *324*, 768−771.
(6) Ohta, T.; Bostwick, A.; Seyller, T.; Horn, K.; Rotenberg, E. Controlling the Electronic Structure of Bilayer Graphene. *Science* **2006**, *313*, 951−954.
(7) Choudhury, D.; Das, B.; Sarma, D. D.; Rao, C. N. R. XPS Evidence for Molecular Charge-Transfer Doping of Graphene. *Chem. Phys. Lett.* **2010**, *497*, 66−69.
(8) Das, B.; Voggu, R.; Rout, C. S.; Rao, C. N. R. Changes in the Electronic Structure and Properties of Graphene Induced by Molecular Charge-Transfer. *Chem. Commun.* **2008**, 5155−5157.
(9) Voggu, R.; Das, B.; Rout, C. S.; Rao, C. N. R. Effects of Charge Transfer Interaction of Graphene with Electron Donor and Acceptor Molecules Examined Using Raman Spectroscopy and Cognate Techniques. *J. Phys.: Condens. Matter* **2008**, *20*, 472204.
(10) Kongraksawech, T.; Vázquez-Landaverde, P.; Huerta-Ruelas, J.; Torres, J. A. Cienc. Ionic Strength and pH Effects on Optical Thermographs for Bovine Serum Albumin (BSA). *Tecnol. Aliment.* **2007**, *5*, 259−264.
(11) Reynaud, J. A.; Malfoy, B.; Bere, A. The Electrochemical Oxidation of Three Proteins: RNAase A, Bovine Serum Albumin and Concanavalin A at Solid Electrodes. *Bioelectrochem. Bioenerg.* **1980**, *7*, 595−606.
(12) Li, B.; Shi, X.; Gu, W.; Zhao, K.; Chen, N.; Xian, Y. Graphene Based Electrochemical Biosensor for Label-Free Measurement of the Activity and Inhibition of Protein Tyrosine Kinase. *Analyst* **2013**, *138*, 7212−7217.
(13) Ostatná, V.; Černocká, H.; Kurzątkowska, K.; Paleček, E. Native and Denatured Forms of Proteins Can Be Discriminated at Edge Plane Carbon Electrodes. *Anal. Chim. Acta* **2012**, *735*, 31−36.
(14) Brabec, V.; Mornstein, V. Electrochemical Behavior of Proteins at Graphite Electrodes, I. Electrooxidation of Proteins as a New Probe of Protein Structure and Reactions. *Biochim. Biophys. Acta* **1980**, *625*, 43−50.
(15) Paleček, E.; Jelen, F.; Teijeiro, C. Biopolymer-Modified Electrodes in the Voltammetric Determination of Nucleic Acids and Proteins at the Submicrogram Level. *Anal. Chim. Acta* **1993**, *273*, 175−186.
(16) Cai, X.; Rivas, G.; Farias, P. A. M.; Shiraishi, H.; Wang, J.; Paleček, E. Potentiometric Stripping Analysis of Bioactive Peptides at Carbon Electrodes Down to Subnanomolar Concentration. *Anal. Chim. Acta* **1996**, *332*, 49−57.
(17) Paleček, E.; Bartošík, M.; Ostatná, V.; Trefulka, M. Electrocatalysis in Proteins, Nucleic Acids and Carbohydrates. *Chem. Record* **2012**, *12*, 27−45.
(18) Kim, K. S.; Um, Y. M.; Jang, J.; Choe, W.-S.; Yoo, P. J. Highly Sensitive Reduced Graphene Oxide Impedance Sensor Harnessing π-Stacking Interaction Mediated Direct Deposition of Protein Probes. *ACS Appl. Mater. Interfaces* **2013**, *5*, 3591−3598.

DOI: 10.1021/am507246v
ACS Appl. Mater. Interfaces 2015, 7, 1250−1256

(19) Li, X.; Cai, W.; An, J.; Kim, S.; Nah, J.; Yang, D.; Piner, R.; Velamakanni, A.; Jung, I.; Tutuc, E.; Banerjee, S. K.; Colombo, L.; Ruoff, R. S. Large-Area Synthesis of High-Quality and Uniform Graphene Films on Copper Foils. *Science* **2009**, *324*, 1312−1314.
(20) Protein 2014. *Encyclopædia Britannica Online*; http://www.britannica.com/EBchecked/topic/479680/protein; retrieved June 26, 2014.
(21) Vigil, G.; Xu, Z.; Steinberg, S.; Israelachvili, J. Interactions of Silica Surfaces. *J. Colloid Interface Sci.* **1994**, *165*, 367−385.
(22) Rezwan, K.; Meier, L. P.; Gauckler, L. Lysozyme and Bovine Serum Albumin Adsorption on Uncoated Silica and AlOOH-Coated Silica Particles: the Influence of Positively and Negatively Charged Oxide Surface Coatings. *J. Biomater.* **2005**, *26*, 4351−4357.
(23) Porath, J.; Sundberg, L.; Fornstedt, N.; Olson, I. Salting-out in Amphiphilic Gels as a New Approach to Hydrophobia Adsorption. *Nature* **1973**, *245*, 465−466.
(24) Shirahama, H.; Suzawa, T. Adsorption of Heat-Denatured Albumin onto Polymer Latices. *J. Colloid Interface Sci.* **1988**, *126*, 269−277.
(25) Leenaerts, O.; Partoens, B.; Peeters, F. M. Water on Graphene: Hydrophobicity and Dipole Moment Using Density Functional Theory. *Phys. Rev. B* **2009**, *79*, 235440.
(26) Ferrari, A. C.; Meyer, J. C.; Scardaci, V.; Casiraghi, C.; Lazzeri, M.; Mauri, F.; Piscanec, S.; Jiang, D.; Novoselov, K. S.; Roth, S.; Geim, A. K. Raman Spectrum of Graphene and Graphene Layers. *Phys. Rev. Lett.* **2006**, *97*, 187401.
(27) Ferrari, A. C. Raman Spectroscopy of Graphene and Graphite: Disorder, Electron−Phonon Coupling, Doping and Nonadiabatic Effects. *Solid State Commun.* **2007**, *143*, 47−57.
(28) Das, A.; Pisana, S.; Chakraborty, B.; Piscanec, S.; Saha, S. K.; Waghmare, U. V.; Novoselov, K. S.; Krishnamurthy, H. R.; Geim, A. K.; Ferrari, A. C.; Sood, A. K. Monitoring Dopants by Raman Scattering in an Electrochemically Top-Gated Graphene Transistor. *Nat. Nanotechnol.* **2008**, *3*, 210−215.
(29) Ni, Z. H.; Wang, H. M.; Luo, Z. Q.; Wang, Y. Y.; Yu, T.; Wu, Y. H.; Shen, Z. X. The Effect of Vacuum Annealing on Graphene. *J. Raman Spectrosc.* **2010**, *41*, 479−483.

DOI: 10.1021/am507246v
ACS Appl. Mater. Interfaces 2015, 7, 1250−1256